

Impact of oxygen annealing on the heat capacity and magnetic resonance of superconducting $\text{Pr}_{0.88}\text{LaCe}_{0.12}\text{CuO}_{4-\delta}$

Shiliang Li,¹ Songxue Chi,¹ Jun Zhao,¹ H.-H. Wen,² M. B. Stone,³ J. W. Lynn,⁴ and Pengcheng Dai^{1,3,*}

¹*Department of Physics and Astronomy, The University of Tennessee, Knoxville, Tennessee 37996-1200, USA*

²*National Laboratory for Superconductivity, Institute of Physics and National Laboratory for Condensed Matter Physics, Chinese Academy of Sciences, P. O. Box 603, Beijing 100080, People's Republic of China*

³*Neutron Scattering Science Division, Oak Ridge National Laboratory, Oak Ridge, Tennessee 37831-6393, USA*

⁴*Center for Neutron Research, National Institute of Standards and Technology, Gaithersburg, Maryland 20899-6102, USA*

(Received 28 April 2008; published 23 July 2008)

We use thermodynamic and neutron-scattering measurements to study the effect of oxygen annealing on the superconductivity and magnetism in $\text{Pr}_{0.88}\text{LaCe}_{0.12}\text{CuO}_{4-\delta}$. Although the transition temperature T_c measured by susceptibility and superconducting coherence length increases smoothly with gradual oxygen removal from the annealing process, bulk superconductivity, marked by a specific-heat anomaly at T_c and the presence of a neutron magnetic resonance, only appears abruptly when T_c is close to the largest value. These results suggest that the effect of oxygen annealing must first be determined in order to establish a Ce doping dependence of antiferromagnetism and superconductivity phase diagram for electron-doped copper oxides.

DOI: 10.1103/PhysRevB.78.014520

PACS number(s): 74.25.Fy, 74.25.Ha

I. INTRODUCTION

High transition temperature (high- T_c) superconductivity occurs in copper oxides when sufficient holes or electrons are doped into the CuO_2 planes of their antiferromagnetic (AF) parent compounds. To understand the relationship between antiferromagnetism and superconductivity, it is essential to determine the doping evolution of the magnetic phase diagram. For hole-doped $\text{La}_{2-x}\text{Sr}_x\text{CuO}_4$ (LSCO), the static long-range AF order is suppressed and superconductivity emerges for a critical Sr doping level of $x > 0.06$.^{1,2} In the case of electron-doped copper oxides such as $\text{Nd}_{2-x}\text{Ce}_x\text{CuO}_{4-\delta}$ (NCCO), $\text{Pr}_{2-x}\text{Ce}_x\text{CuO}_{4-\delta}$ (PCCO), and $\text{Pr}_{1-x}\text{LaCe}_x\text{CuO}_{4-\delta}$ (PLCCO), the long-range AF phase appears to extend over a wide Ce doping range ($x \geq 0.1$) and coexist with superconductivity.^{3,4} In particular, transport^{5,6} and optical⁷ measurements on PCCO thin films revealed an AF quantum critical point (QCP) inside the superconducting dome at $x \approx 0.16$, where the coexisting AF and superconducting phase ($0.13 \leq x \leq 0.16$) is separated from the pure superconducting phase ($x > 0.16$). These results are consistent with the presence of a normal-state gap (induced by the static/fluctuating AF order) at $x = 0.15$ on NCCO revealed by angle-resolved photoemission spectroscopy⁸ and optical measurements.⁹ However, a recent neutron-scattering experiment on NCCO suggests that genuine long-range AF order and superconductivity do not coexist, and the QCP separating the pure AF and superconducting phases lies just before the superconducting dome at $x \approx 0.13$.¹⁰ Therefore, the true AF phase in NCCO extends only to $x \approx 0.13$ and the phase diagrams of electron-doped materials are much different from previous work,³⁻⁷ as illustrated in the inset of Fig. 1(a).

Unlike their hole-doped counterparts, electron-doped materials exhibit no superconductivity in the as-grown state until they are annealed in an oxygen-poor environment to remove a small amount of oxygen.^{11,12} Although three-dimensional (3D) static long-range AF order is observed to coexist with superconductivity in annealed NCCO for

$0.13 \leq x \leq 0.17$,^{3,4} the existence of static AF order has been argued as an artifact induced by the inhomogeneous annealing process for this family of materials.¹⁰ Therefore, to understand the microscopic mechanism of the annealing process and its impact on bulk superconductivity,¹³⁻¹⁵ one must choose electron-doped materials that can be annealed continuously into pure superconductors without coexisting static AF order.^{16,17} Our prior elastic neutron-scattering measurements showed that electron-doped PLCCO ($x = 0.12$) is ideal for this purpose.¹⁸

In this paper, we present systematic specific-heat and neutron-scattering measurements designed to study the annealing effect on PLCCO ($x = 0.12$) as the system is tuned from an as-grown antiferromagnet to a pure superconductor ($T_c = 27$ K) without static AF order. Although magnetic susceptibility and elastic neutron-scattering measurements suggest a gradually increasing T_c (Fig. 1) and decreasing T_N , respectively, with increasing oxygen loss,¹⁸ we find that the bulk superconductivity and neutron magnetic resonance¹⁹ occur only for PLCCO samples with the largest T_c 's. Our results thus suggest that the neutron-scattering results determined using NCCO single crystals without systematically studying the oxygen annealing effect is unreliable,¹⁰ and the phase diagram obtained on PCCO films with properly tuned optimal superconductivity^{5,6} reveals the intrinsic properties of the electron-doped materials.

II. EXPERIMENT

We grew PLCCO ($x = 0.12$) single crystals by the traveling-solvent floating-zone method.¹⁸ The as-grown non-superconducting PLCCO exhibits static AF order with $T_N \sim 200$ K.¹⁸ The annealing process is a dynamic process of removing oxygen, and the final oxygen content is determined by the temperature, the oxygen partial pressure, and the annealing time.^{16,17} Instead of annealing in argon gas,⁴ we use high-vacuum annealing to reduce the oxygen partial pressure and increase the dynamic range of temperature.¹⁶

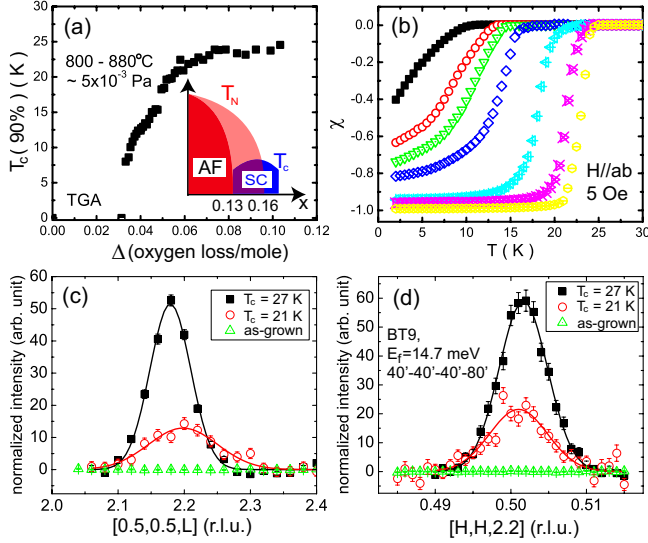


FIG. 1. (Color online) (a) T_c (90%) vs Δ for the same sample annealed at various temperatures in vacuum. T_c (90%) is defined as the temperature where the susceptibility loses 90% of its value at 2 K. The inset shows the schematic Ce content dependence of T_N and T_c . (b) Magnetic susceptibility of PLCCO samples with $\delta=0.034, 0.038, 0.042, 0.047, 0.053, 0.066, 0.092$ from left to right of the figure. (c) and (d) are the $[0.5, 0.5, L]$ and $[H, H, 2.2]$ scans through the impurity phase R_2O_3 peak position. The scattering intensity is normalized to a measured phonon at $Q=(-0.1, -0.1, 6)$ and $T=80$ K (Ref. 26).

Figure 1(a) shows T_c vs oxygen loss Δ obtained for one PLCCO crystal (~ 1 gram) using a thermogravimetric analyzer (TGA) at temperatures from 800 to 880 °C. Data points correspond to sequential days of annealing. Magnetic susceptibility measurements in Fig. 1(b) show that the superconducting volume fraction becomes larger than 90% for samples with $T_c \geq 20$ K. Our neutron-scattering experiments were carried out on the HB-1 and BT-9 thermal triple-axis spectrometers at the high-flux isotope reactor, Oak Ridge National Laboratory and NIST Center for Neutron Research, respectively. We define the wave vector Q at (q_x, q_y, q_z) as $(H, K, L) = (q_x a/2\pi, q_y a/2\pi, q_z c/2\pi)$ reciprocal lattice unit (r.l.u.) in the tetragonal unit cell of PLCCO (space group $I4/mmm$, $a=b=3.98$ Å, and $c=12.28$ Å). For the specific-heat measurements, we used a commercial calibrated calorimeter with a 14 T physical property measurement system and a ^3He insert capable of reaching 0.4 K.

Recently, we suggested that the annealing process in electron-doped cuprates mainly involves repairing Cu deficiencies in the as-grown sample,¹⁵ which suppresses local superconductivity and induces staggered AF moments extending over several unit cells much like the effect of nonmagnetic Zn impurities.^{20,21} As a consequence, the band filling and band parameters are not much affected by the annealing process.^{14,22} Assuming that the annealing process indeed fills the copper vacancies by producing thin slabs of the anion-deficient fluorite impurity phase R_2O_3 ($R=\text{Pr, La, Ce}$) through $R_2Cu_{1-f}O_{4-\delta} = (1-f)(R_2CuO_{4-\beta}) + f(R_2O_3) + [-\delta + \beta + f(1-\beta)](O)$ where oxygen loss $\Delta = -\delta + \beta + f(1-\beta)$,¹⁵ the amount of the impu-

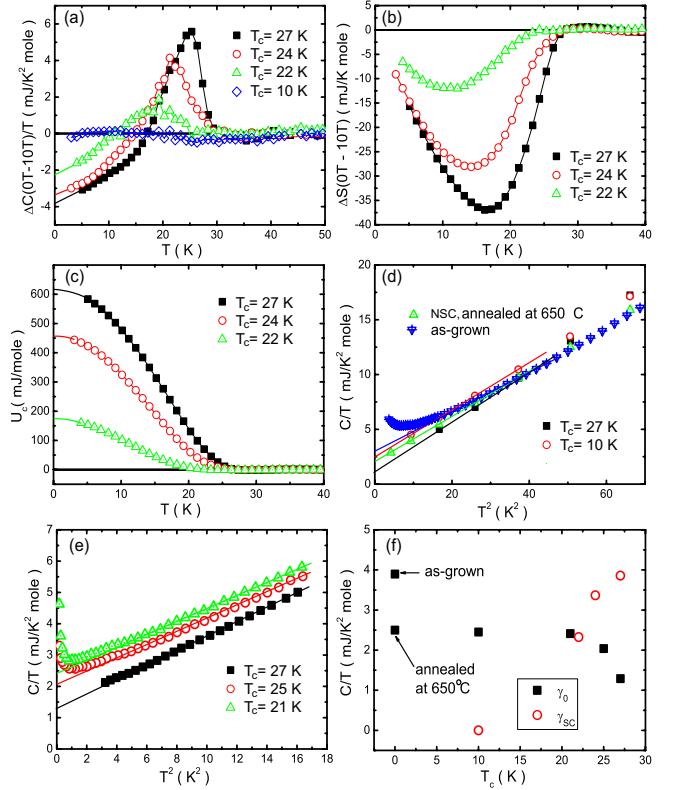


FIG. 2. (Color online) (a) The subtracted electronic specific heat for four different samples with field $H\parallel c$. A small linear background (<0.35 mJ/K² mole at 30 K) is also subtracted for all the samples. (b) The entropy difference between the superconducting and normal states of three different T_c PLCCO. (c) The temperature dependence of U_c for three different samples. (d) Temperature dependence of C/T . (e) C/T vs T^2 measured on He³ probe. (f) The residual electronic specific heat $C = \gamma_0 T$ at 0 K and the superconducting electronic specific heat $C = \gamma_{SC} T$ at 0 K.

urity R_2O_3 created during the annealing process should increase with increasing Δ . Figures 1(c) and 1(d) show the $[0.5, 0.5, L]$ and $[H, H, 2.2]$ scans through the R_2O_3 impurity peak position at $(0.5, 0.5, 2.2)$ respectively.^{23,24} These data reveal that the impurity peaks for the higher T_c samples have a larger peak intensity and narrower peak width along the L -axis direction. The volume fraction of the impurity phase increases with increasing Δ . Quantitatively, we estimate that the ratio of impurity contents between the $T_c=27$ K and 21 K samples is about 1.6, meaning that the $T_c=21$ K sample should have $\sim 0.75\%$ Cu vacancies if we assume that the $T_c=27$ K PLCCO has no Cu deficiency.¹⁵

Although Figs. 1(a) and 1(b) show that the T_c of PLCCO measured by susceptibility increases with increasing Δ , it is unclear when bulk superconductivity first appears in the annealing process. Electronic specific-heat measurements are one way to determine bulk superconductivity. Since the upper critical field H_{c2} of electron-doped superconductors is less than 10 T for $H\parallel c$, the change in the electronic specific heat can be obtained from the difference between specific heats in the superconducting ($H=0$ T) and field-suppressed normal states ($H=10$ T).²⁵ Figure 2(a) shows that the superconducting jump decreases rapidly with decreasing T_c and

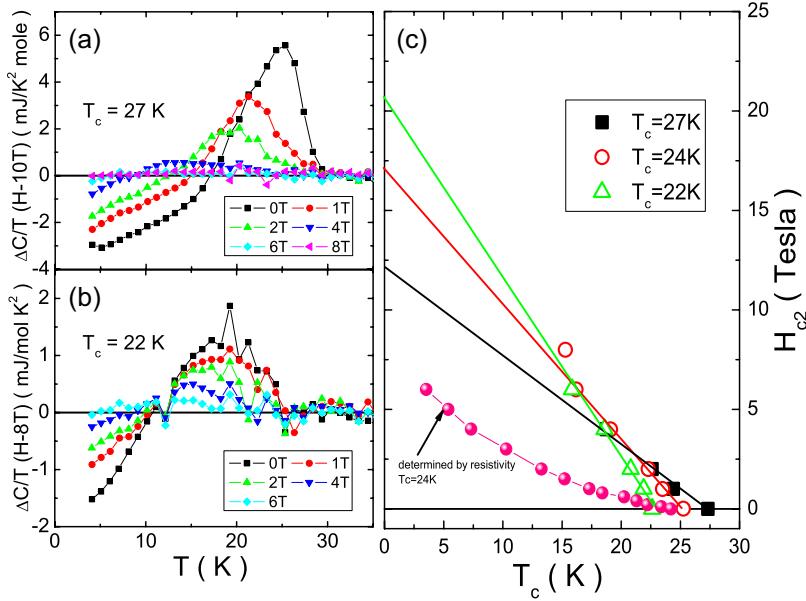


FIG. 3. (Color online) Magnetic-field dependence of the superconducting heat capacity anomalies for (a) $T_c=27$ K and (b) 22 K PLCCO samples. (c) A comparison of the upper critical field H_{c2} determined by specific-heat measurements for various T_c PLCCO samples. $C(T)$ for $T_c=24$ K sample has already been published elsewhere (Ref. 26). For comparison, the H_{c2} of the $T_c=24$ K sample obtained from resistivity is also shown. The solid linear lines are guides for the eyes.

vanishes for $T_c < 20$ K samples, although the superconducting volume determined by magnetic susceptibility is still large. Figures 2(b) and 2(c) plot the differential entropy ΔS and the superconducting condensation energy U_c using $\Delta S(T) = \int_0^T \frac{C_{sc} - C_n}{T'} dT'$, $U_c(T) = \int_{T_c}^T (\Delta S(T')) dT'$,²⁶ which further illustrates how fast the bulk superconductivity disappears with decreasing T_c .

To extract the absolute values of the electronic specific heat, we fit the low-temperature total specific-heat data as $C_{\text{total}}/T = \gamma_0 + \beta T^2$, where βT^2 is the lattice contribution and $\gamma_0 T$ represents the electronic contribution. For as-grown PLCCO, the large low-temperature Schottky anomaly prevents an accurate determination of γ_0 . For annealed nonsuperconducting and superconducting samples, we obtain γ_0 using data in Figs. 2(d) and 2(e) and a measure of the residual superconducting contribution, γ_{sc} , using data in Fig. 2(a) with $\Delta C/T(10 \text{ T} - 0 \text{ T})$. The T_c dependences of γ_0 and γ_{sc} are shown in Fig. 2(f). The nonzero γ_0 may arise from the residual metallic nonsuperconducting portion of the superconductor.²⁵ Previous experiments have shown the existence of static 3D AF order coexisting with superconductivity in lower T_c samples.¹⁸ If a low- T_c PLCCO sample is electronically phase-separated into insulating AF ordered, metallic nonsuperconducting, and superconducting regions,¹⁸ one would expect that the residual γ_0 associated with the nonsuperconducting part of the metallic phase decreases with increasing $U_c(0)$ and volume fraction. In this picture, the annealing process initially weakens the static AF order with almost no change in the metallic phase, as indicated by the reduction in γ_0 from the as-grown to 650 °C annealed nonsuperconducting states [Fig. 2(f)]. Bulk superconductivity only emerges for PLCCO with $T_c \geq 20$ K. With further annealing, γ_{sc} increases rapidly with increasing T_c and U_c while γ_0 decreases slowly, suggesting that the enhanced superconductivity with annealing is at the expense of static AF order. For PLCCO samples with $T_c \geq 24$ K, where the static AF order essentially vanishes,¹⁹ the increasing U_c with annealing may be at the expense of the metallic nonsupercon-

ducting phase with a reduction in γ_0 [Fig. 2(f)].

Figures 3(a) and 3(b) show the magnetic-field dependence of the superconducting specific-heat anomaly for the $T_c=27$ and 22 K samples, respectively. Figure 3(c) plots the temperature dependence of H_{c2} determined by the middle point of the negative slope region in the specific-heat jump. Using the Helfand-Werthamer formula $H_{c2}(0) \approx 0.7 \times T_c \times dH_{c2}/dT$,²⁷ we find the $H_{c2}(0)$ values of 8.5 T, 12 T, and 15 T for $T_c=27$ K, 24 K, and 22 K, respectively.^{28–30} For pure superconducting $T_c=27$ K PLCCO, the in-plane coherence length $\xi(0)$ is about 62 Å in the clean *s*-wave limit,^{28,31} where $H_{c2}(0) = \phi_0/2\pi\xi^2(0)$ and ϕ_0 is the quantum of flux. For $T_c=24$ K and 22 K samples, $\xi(0)$ decreases to 52 Å and 47 Å, respectively. This is consistent with the expected 0.75% Cu vacancies in the $T_c=21$ K sample, where the average distance between two Cu vacancies is about 50 Å. On the other hand, dynamic spin-spin correlations at $\hbar\omega=1.5$ meV decreases with increasing T_c , changing from 200 ± 21 Å to 93 ± 14 Å and 80 ± 10 Å for $T_c=21$ K and $T_N=40$ K, $T_c=23$ K and $T_N=25$ K, and $T_c=24$ K PLCCO, respectively.¹⁸ Therefore, oxygen annealing should affect spin correlations determined by two-axis measurements.¹⁰

To test if the annealing process also affects the recently discovered magnetic resonance,¹⁹ we carried out neutron-scattering experiments on $T_c=27$ K and $T_c=21$ K samples. Similar to measurements on $T_c=24$ K samples,¹⁹ we isolate the resonance (E_r) by taking the difference of constant- Q scans at $Q=(0.5, 0.5, 0)$ between the superconducting ($T=6$ K) and normal states ($T=30$ K). The data of constant- Q scans for the $T_c=27$ K and $T_c=21$ K samples are shown in Figs. 4(a) and 4(b), respectively. By fitting the subtracted data with Gaussians, we find $E_r=10.3 \pm 0.38$ meV [Fig. 4(c)] and $E_r=9.3 \pm 0.69$ meV [Fig. 4(d)]. The decreasing energy E_r of the resonance with decreasing T_c is consistent with the reduction of the superconducting gap³¹ and the $E_r=5.8k_B T_c$ universal plot.¹⁹ Figures 4(e) and 4(f) show constant energy scans near E_r at 6 K and 30 K for these two samples. Comparison of these data

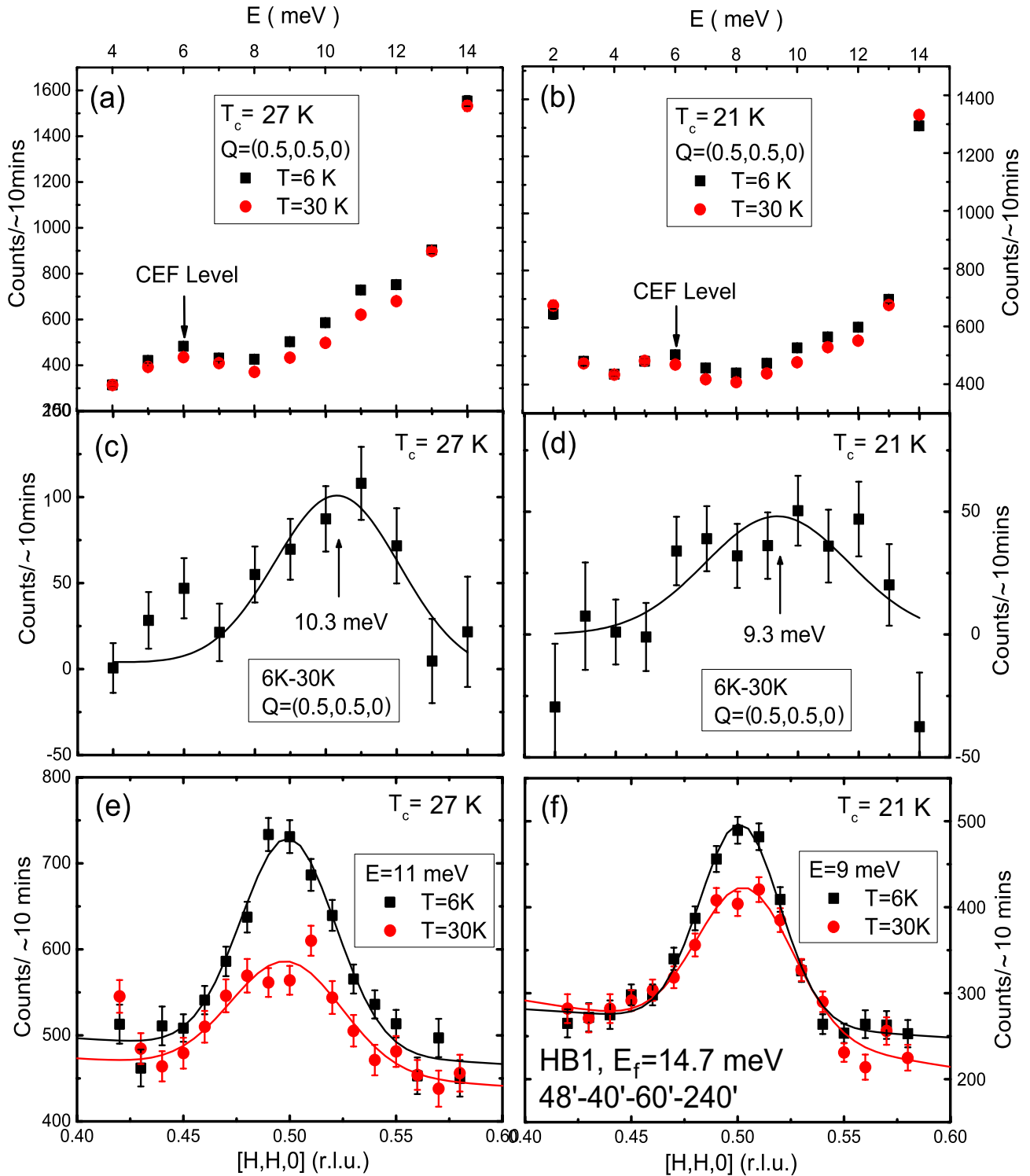


FIG. 4. (Color online) Constant Q scans at $Q=(0.5,0.5,0)$ at $T=6$ K and 30 K for (a) $T_c=27$ K and (b) $T_c=21$ K PLCCO. The small peak at $\hbar\omega=6$ meV is the Pr crystal field from the “impurity” R_2O_3 phase which is not present in the as-grown PLCCO (Ref. 19). The corresponding differences between 6 K and 30 K are shown in (c) and (d), indicating resonance peaks. (e) and (f) show constant energy scans through $[H,H,0]$ at 6 K and 30 K near the resonance energies for these two samples.

also reveals that the intensity gain from the normal to superconducting states for the $T_c=27$ K sample is considerably larger than that of the $T_c=21$ K sample in agreement with our conclusions regarding bulk superconductivity based on thermodynamic measurements.

III. DISCUSSIONS AND CONCLUSIONS

The effect of annealing on superconductivity and magnetism in PLCCO appears to be similar to that of Zn doping in the electron-doped superconductor NCCO, where a few per-

cent of Zn impurities (Cu vacancies in the as-grown sample) can completely suppress superconductivity.^{20,21} In addition, the increasing γ_0 with decreasing T_c in PLCCO [Fig. 2(f)] is also similar to the Zn doping dependence of γ_0 in YBCO.³² Since both the superconducting coherence length and spin-spin correlation length are strongly affected by the oxygen annealing process, these results call into question the suggestion that there is no genuine coexisting AF and superconducting phase and the QCP occurs just before the superconducting dome at $x \approx 0.13$.¹⁰ In our view, any attempt to establish the Ce doping evolution of the AF to superconducting phase transition on electron-doped materials must begin by systematically determining the oxygen annealing effect at different Ce dopings.³³ This implies that one must examine the

electron-doped superconductors with the highest T_c at a fixed Ce doping as in the thin-film PCCO case to determine their intrinsic electronic properties.^{5,6}

ACKNOWLEDGMENTS

The neutron-scattering work was supported in part by the U.S. NSF Grant No. DMR-0756568. The PLCCO single-crystal growth at UT was supported by the U.S. DOE BES under Grant No. DE-FG02-05ER46202. ORNL was supported by the U.S. DOE under Contract No. DE-AC-05-00OR22725 through UT/Battell, LLC. Work at IOP was supported by CAS ITSNEP Projects No. 2006CB601000 and No. 2006CB92180.

*daip@ornl.gov

- ¹M. A. Kastner, R. J. Birgeneau, G. Shirane, and Y. Endoh, *Rev. Mod. Phys.* **70**, 897 (1998).
- ²S. Wakimoto, G. Shirane, Y. Endoh, K. Hirota, S. Ueki, K. Yamada, R. J. Birgeneau, M. A. Kastner, Y. S. Lee, P. M. Gehring, and S. H. Lee, *Phys. Rev. B* **60**, R769 (1999).
- ³T. Uefuji, K. Kurahashi, M. Fujita, M. Matsuda, and K. Yamada, *Physica C* **378-381**, 273 (2002).
- ⁴M. Fujita, T. Kubo, S. Kuroshima, T. Uefuji, K. Kawashima, K. Yamada, I. Watanabe, and K. Nagamine, *Phys. Rev. B* **67**, 014514 (2003).
- ⁵Y. Dagan, M. M. Qazilbash, C. P. Hill, V. N. Kulkarni, and R. L. Greene, *Phys. Rev. Lett.* **92**, 167001 (2004).
- ⁶W. Yu, J. S. Higgins, P. Bach, and R. L. Greene, *Phys. Rev. B* **76**, 020503(R) (2007).
- ⁷A. Zimmers, J. M. Tomczak, R. P. S. M. Lobo, N. Bontemps, C. P. Hill, M. C. Barr, Y. Dagan, R. L. Greene, A. J. Millis, and C. C. Homes, *Europhys. Lett.* **70**, 225 (2005).
- ⁸H. Matsui, T. Takahashi, T. Sato, K. Terashima, H. Ding, T. Uefuji, and K. Yamada, *Phys. Rev. B* **75**, 224514 (2007).
- ⁹Y. Onose, Y. Taguchi, K. Ishizaka, and Y. Tokura, *Phys. Rev. B* **69**, 024504 (2004).
- ¹⁰E. M. Motoyama, G. Yu, I. M. Vishik, O. P. Vajk, P. K. Mang, and M. Greven, *Nature (London)* **445**, 186 (2007).
- ¹¹Y. Tokura, H. Takagi, and S. Uchida, *Nature (London)* **337**, 345 (1989).
- ¹²H. Takagi, S. Uchida, and Y. Tokura, *Phys. Rev. Lett.* **62**, 1197 (1989).
- ¹³J. S. Higgins, Y. Dagan, M. C. Barr, B. D. Weaver, and R. L. Greene, *Phys. Rev. B* **73**, 104510 (2006).
- ¹⁴J. Gauthier, S. Gagné, J. Renaud, M. È. Gosselin, P. Fournier, and P. Richard, *Phys. Rev. B* **75**, 024424 (2007).
- ¹⁵H. J. Kang, Pengcheng Dai, B. J. Campbell, P. J. Chupas, S. Rosenkranz, P. L. Lee, Q. Huang, S. L. Li, S. Komiyama, and Y. Ando, *Nat. Mater.* **6**, 224 (2007).
- ¹⁶J. S. Kim and D. R. Gaskell, *Physica C* **209**, 381 (1993).
- ¹⁷W. Jiang, S. N. Mao, X. X. Xi, X. Jiang, J. L. Peng, T. Venkatesan, C. J. Lobb, and R. L. Greene, *Phys. Rev. Lett.* **73**, 1291 (1994).
- ¹⁸Pengcheng Dai, H. J. Kang, H. A. Mook, M. Matsuura, J. W. Lynn, Y. Kurita, S. Komiyama, and Y. Ando, *Phys. Rev. B* **71**, 100502(R) (2005); S. D. Wilson, S. L. Li, Pengcheng Dai, W. Bao, J. H. Chung, H. J. Kang, S. H. Lee, S. Komiyama, Y. Ando, and Q. Si, *ibid.* **74**, 144514 (2006).
- ¹⁹S. D. Wilson, Pengcheng Dai, S. L. Li, S. X. Chi, H. J. Kang, and J. W. Lynn, *Nature (London)* **442**, 59 (2006).
- ²⁰J. M. Tarascon, E. Wang, S. Kivelson, B. G. Bagley, G. W. Hull, and R. Ramesh, *Phys. Rev. B* **42**, 218 (1990).
- ²¹J. Sugiyama, S. Tokuono, S. I. Koriyama, H. Yamauchi, and S. Tanaka, *Phys. Rev. B* **43**, 10489 (1991).
- ²²P. Richard, M. Neupane, Y.-M. Xu, P. Fournier, S. Li, Pengcheng Dai, Z. Wang, and H. Ding, *Phys. Rev. Lett.* **99**, 157002 (2007).
- ²³M. Matsuura, Pengcheng Dai, H. J. Kang, J. W. Lynn, D. N. Argyriou, K. Prokes, Y. Onose, and Y. Tokura, *Phys. Rev. B* **68**, 144503 (2003).
- ²⁴P. K. Mang, S. Larochelle, A. Mehta, O. P. Vajk, A. S. Erickson, L. Lu, W. J. L. Buyers, A. F. Marshall, K. Prokes, and M. Greven, *Phys. Rev. B* **70**, 094507 (2004).
- ²⁵H. Balci and R. L. Greene, *Phys. Rev. B* **70**, 140508(R) (2004).
- ²⁶S. D. Wilson, S. L. Li, J. Zhao, G. Mu, H.-H. Wen, J. W. Lynn, P. G. Freeman, L. P. Regnault, K. Habicht, and Pengcheng Dai, *Proc. Natl. Acad. Sci. U.S.A.* **104**, 15259 (2007).
- ²⁷E. Helfand and N. R. Werthamer, *Phys. Rev.* **147**, 288 (1966).
- ²⁸P. Fournier and R. L. Greene, *Phys. Rev. B* **68**, 094507 (2003).
- ²⁹H. Balci, C. P. Hill, M. M. Qazilbash, and R. L. Greene, *Phys. Rev. B* **68**, 054520 (2003).
- ³⁰Y. Wang, S. Ono, Y. Onose, G. Gu, Y. Ando, Y. Tokura, S. Uchida, and N. P. Ong, *Science* **299**, 86 (2003).
- ³¹L. Shan, Y. Huang, Y. L. Wang, S. L. Li, J. Zhao, Pengcheng Dai, Y. Z. Zhang, C. Ren, and H. H. Wen, *Phys. Rev. B* **77**, 014526 (2008).
- ³²D. L. Sisson, S. G. Doettinger, A. Kapitulnik, R. Liang, D. A. Bonn, and W. N. Hardy, *Phys. Rev. B* **61**, 3604 (2000).
- ³³Y. Tanaka, T. Motohashi, M. Karppinen, and H. Yamauchi, *J. Solid State Chem.* **181**, 365 (2008).